Inorganic Chemistry

Article

pubs.acs.org/IC

Cu_4I_4 Clusters Supported by P^N-type Ligands: New Structures with Tunable Emission Colors

Zhiwei Liu, Peter I. Djurovich, Matthew T. Whited, and Mark E. Thompson*

Department of Chemistry, University of Southern California, Los Angeles, California 90089, United States

Supporting Information

ABSTRACT: A series of Cu_4I_4 clusters (**1**−**5**) supported by two P^N-type ligands 2-[(di**R**phosphino)methyl]pyridine (**1**, R = phenyl; **2**, R = cyclohexyl; **3**, R = *tert*-butyl; **4**, R = *iso*-propyl; **5**, R = ethyl) have been synthesized. Single crystal X-ray analyses show that all five clusters adopt a rare "octahedral" geometry. The central core of the cluster consists of the copper atoms arranged in a parallelogram with μ^4-iodides above and below the copper plane. The copper atoms on the two short edges of the parallelogram (Cu−Cu = 2.525(2)−2.630(1) Å) are bridged with μ^2-iodides, whereas the long edges (Cu−Cu = 2.839(3)−3.035(2) Å) are bridged in an antiparallel fashion by the P^N ligands. This Cu_4I_4 geometry differs significantly from the "cubane" and "stairstep" geometries reported for other $Cu_4I_4L_4$ clusters. Luminescence spectra of clusters **3** and **4** display a single emission around 460 nm at room temperature that is assigned to emission from a triplet halide-to-ligand charge-transfer (^{3}XLCT) excited state, whereas clusters **1**, **2**, and **5** also have a second band around 570 nm that is assigned to a Cu_4I_4 cluster-centered (^{3}CC) excited state. The structural and photophysical properties of a dinuclear $Cu_2I_2(P^N)_2$ complex obtained during the sublimation of cluster **3** is also provided.

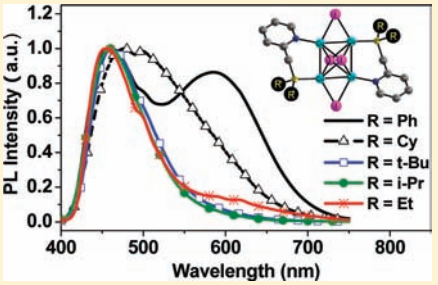

INTRODUCTION

Copper(I) complexes have attracted considerable interest because of their rich structural and photophysical properties[1−3] and potential applications as inexpensive, abundant materials in optoelectronics,[4,5] catalysis,[6,7] and biological systems.[8] In particular, complexes based on copper(I) iodide and pyridine (py) ligands display remarkable structural diversity. For example, complexes with nuclearities ranging from monometallic (e.g., $CuI(3\text{-Mepy})_3$ (3-Mepy = 3-methylpyridine)) to polymetallic (e.g., $(CuIpy)_\infty$) have been prepared from the simple combination of copper(I) iodide and pyridine-type ligands in different ratios, although the most common are bimetallic ($Cu_2I_2L_4$), tetrametallic ($Cu_4I_4L_4$), and polymeric ($(CuIL)_\infty$) clusters.[9−12] Among these complexes, $Cu_4I_4L_4$ clusters have been extensively investigated because of their peculiar photoluminescence properties.[1,13−17]

The most common motif for $Cu_4I_4L_4$ clusters reported in the literature is a cubane-like structure consisting of a copper tetrahedron with iodides capping the four faces (Figure 1b). This geometry can also be viewed as a pair of Cu_2I_2 fragments with their Cu−Cu axes oriented perpendicular to each other (Figure 1a). Generally, the cubane cluster exhibits two distinct emission bands, one at high energy (ca. 450 nm) and the other at low energy (ca. 600 nm), arising from halide-to-ligand charge-transfer (^{3}XLCT) excited states and triplet cluster-centered (^{3}CC), respectively.[18−20] The former band is quite prominent at low temperature and is strongly influenced by the electronic structure of ligand. The latter band dominates at room temperature in clusters with Cu−Cu distances less than 2.8 Å (the van der Waals radii of Cu is 1.4 Å,[21] although it is noteworthy that the value was recently re-evaluated to be 1.92 Å[22−24]).

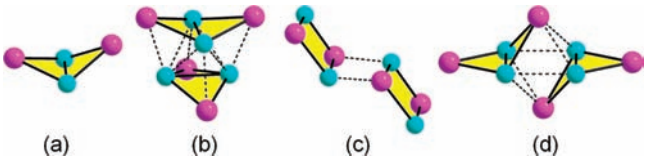

Figure 1. Illustrations of the copper iodide cores of (a) Cu_2I_2 cluster, (b) cubane-like Cu_4I_4 cluster, (c) repeat unit of a stairstep $(CuIL)_\infty$ cluster, and (d) a new type of Cu_4I_4 cluster, based on crystallographic structural data, Cu, cyan; I, purple. The solid lines show the bonding within the Cu_2I_2 fragment, and the dashed lines in (b), (c), and (d) illustrate the bonding between Cu_2I_2 fragments (based on close atom−atom contacts in the crystal structures).

The $Cu_4I_4L_4$ cluster has also been found in a "stairstep" or "distorted stairstep" configuration, a motif constructed from the association of two Cu_2I_2 fragments along Cu−I edges (Figure 1c).[25−36] In the stairstep structure, Cu−Cu distances are typically longer than 2.8 and hence there are no substantial interactions between Cu ions. Thus, such stairstep complexes exhibit luminescence only from the ^{3}XLCT excited state. Although $Cu_4I_4L_4$ clusters with distorted stairstep structures and short Cu−Cu distances in the 2.65−2.8 Å range have been described in the literature,[25−29] no reports of emission with ^{3}CC characteristics have appeared for these derivatives.

Received: July 18, 2011
Published: December 1, 2011

   dx.doi.org/10.1021/ic2015226 | *Inorg. Chem.* 2012, 51, 230−236

In this paper, we report a series of $Cu_4I_4(P^{\wedge}N)_2$ clusters, supported by bridging 2-[(diorganophosphino)methyl]pyridine ($P^{\wedge}N$) ligands, that have a rare "octahedral" geometry. This structure can be thought of as being built by association of two Cu_2I_2 fragments along $\overline{Cu{-}Cu{-}I}$ faces, leading to a parallel orientation of the Cu−Cu axes in the two fragments (Figure 1d). This geometric arrangement differs significantly from the aforementioned cubane and stairstep $Cu_4I_4L_4$ clusters. Both short (2.52−2.63 Å) and long (2.84−3.04 Å) Cu−Cu interactions are found in these clusters. In the solid state at room temperature, it is found that the emission color of these $Cu_4I_4(P^{\wedge}N)_2$ clusters can be tuned from blue to white by altering the organic groups on the phosphine moiety in the $P^{\wedge}N$ ligand.

EXPERIMENTAL SECTION

General Procedures. Chemicals were received from commercial resources (i.e., CuI and *n*-BuLi were purchased from Aldrich, chlorodiorganophosphines were purchased from TCI) and used as received. Solvents were degassed prior to use, and tetrahydrofuran (THF) was additionally dried over sodium and distilled. All reactions were performed under N_2 atmosphere. ^{1}H NMR spectrum was recorded on a Varian-400MR NMR spectrometer. Chemical shift data for each signal are reported in ppm units with $CDCl_3$ as reference, where δ ($CDCl_3$) = 7.26 ppm. Elemental analyses were performed by the SCS Microanalysis Laboratory at the University of Illinois using a Model CE 440 CHN Analyzer.

Synthesis of $P^{\wedge}N$-Type Ligands. The $P^{\wedge}N$-type ligands were synthesized as shown in Scheme 1, similar to the literature procedure.[37,38] To a stirred solution of 2-picoline (0.93 g, 10 mmol) in THF (30 mL) was added dropwise *n*-BuLi (1.6 M in hexanes, 6.25 mL, 10 mmol) at −78 °C. The mixture was allowed to warm to room temperature for 2 h and then cooled to −78 °C, followed by slow addition of R_2PCl (10 mmol) in THF (10 mL). The mixture was stirred overnight at room temperature. Degassed water (30 mL) was added, though the water did not mix with the THF because of the high concentration of LiCl. The organic layer was separated and dried with Na_2SO_4. The THF was removed by distillation under reduced pressure, and the resulting oily compound was dissolved in 5 mL of degassed CH_2Cl_2. The ligands were used in the next reaction step without further purification.

Scheme 1. Synthesis of $P^{\wedge}N$-Type Ligands and Corresponding Cu_4I_4 Clusters 1−5

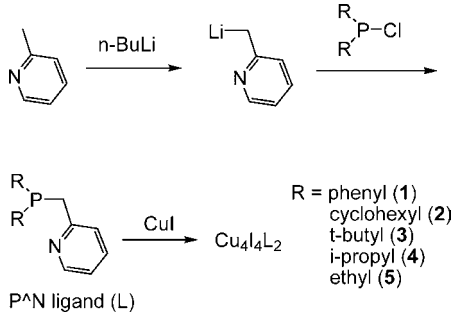

Synthesis of Clusters 1−5. Solutions of CuI in CH_3CN and $P^{\wedge}N$-type ligand in CH_2Cl_2 were filtered through syringe filter (0.45 μm) and the two solutions mixed. The molar ratio of CuI to $P^{\wedge}N$ ligand was 4: 1. The solutions were left standing at room temperature. Clusters were obtained as crystals in times ranging from hours to several days with yields averaging 30% over the two steps (based on 2-picoline). Cluster **1**: Pale yellow crystals (43%) were obtained in 12 h; Anal. Calcd. for $C_{36}H_{32}Cu_4I_4N_2P_2$: C, 32.85; H, 2.45; N, 2.13. Found: C, 32.78; H, 2.09; N, 2.10. Cluster **2**: Yellow crystals (31%) were obtained in 6 h; Anal. Calcd. for $C_{36}H_{56}Cu_4I_4N_2P_2$: C, 32.25; H, 4.21; N, 2.09. Found: C, 32.27; H, 4.16; N, 2.33. Cluster **3**: Pale yellow crystals (28%) were obtained in 3 h; Anal. Calcd. for $C_{28}H_{48}Cu_4I_4N_2P_2$: C, 27.20; H, 3.91; N, 2.27. Found: C, 27.26; H, 3.74; N, 2.24. Cluster **4**: Pale yellow crystals (30%) were obtained in 3 h; Anal. Calcd. for $C_{24}H_{40}Cu_4I_4N_2P_2$: C, 24.42; H, 3.42; N, 2.37. Found: C, 24.53; H, 3.13; N, 2.41. Cluster **5**: White crystals (17%) were obtained in 2 days; ^{1}H NMR (400 MHz, $CDCl_3$): δ 9.06 (d, J = 5.2 Hz, 2H), 7.72 (t, J = 8.0 Hz, 2H), 7.30 (t, J = 7.6 Hz, 2H), 7.21 (d, J = 7.6 Hz, 2H), 3.53 (d, J = 7.2 Hz, 4H), 1.73 (m, 8H), 1.15 (m, 12H). Anal. Calcd. for $C_{20}H_{32}Cu_4I_4N_2P_2$: C, 21.37; H, 2.87; N, 2.49. Found: C, 21.39; H, 2.55; N, 2.45.

Synthesis of Complex 3a. The complex **3a** was obtained by gradient sublimation of the cluster **3** under high temperature (∼ 200 °C) and low pressure (10^{-6} Torr). Yield: ca. 20%. ^{1}H NMR (400 MHz, $CDCl_3$): δ 8.91 (d, J = 4.8 Hz, 2H), 7.68 (t, J = 7.6 Hz, 2H), 7.32 (d, J = 8.0 Hz, 2H), 7.25 (t, J = 6.0 Hz, 2H), 3.23 (d, J = 7.6 Hz, 4H), 1.28 (d, J = 13.6 Hz, 36H). ^{31}P NMR (400 MHz, $CDCl_3$): δ 28.4. Anal. Calcd. for $C_{28}H_{48}Cu_2I_2N_2P_2$: C, 39.31; H, 5.66; N, 3.27. Found: C, 39.37; H, 5.64; N, 3.28.

X-ray Crystallography. Clusters **1**−**5** and complex **3a** were obtained as crystals and found suitable for X-ray measurement. The crystals were mounted on a glass fiber with Paratone-N oil. X-ray diffraction data were collected on a Bruker SMART APEX diffractometer using graphite-monochromated Mo Kα radiation, and structures were determined using direct methods with standard Fourier techniques using the Bruker AXS software package. In some cases, Patterson maps were used in place of the direct methods procedure. Detailed crystal parameters and structure refinements are given in the Supporting Information.

Photophysical Measurements. Photoluminescence spectra were measured using a PTI QuantaMaster model C-60SE spectrophotometer equipped with a 928 PMT detector. Phosphorescent lifetimes were measured by time-correlated single-photon counting using an IBH Fluorocube instrument equipped with a 331 nm LED excitation source. Quantum yield measurements were carried out using a Hamamatsu C9920 system equipped with a xenon lamp, calibrated integrating sphere and model C10027 photonic multichannel analyzer.

Computational Methods. All of the molecular orbital calculations were performed with the Titan (version 1.0.7) software package at the B3LYP level using a LACVP** basis set. Geometric coordinates taken from X-ray crystal structures were used for single-point, density functional theory (DFT) calculations.

RESULTS AND DISCUSSION

The $P^{\wedge}N$-type ligands were synthesized from a reaction of lithio-2-picoline (obtained by metalation of 2-methylpyridine) with chlorodiorganophosphine using a modified literature procedure.[37,38] Considering that $P^{\wedge}N$-type compounds are readily oxidized in air,[39] the ligands were used directly without further purification in the subsequent reaction. The five clusters **1**−**5** were obtained as pale yellow to yellow crystals that precipitated from mixed solutions (CuI in CH_3CN and ligand in CH_2Cl_2) over a period of hours to days. Clusters **1**−**4** are poorly soluble in common solvents (toluene, CH_2Cl_2, THF), whereas **5** is soluble enough that NMR spectra can be obtained in $CDCl_3$.

Samples of **1**−**5** isolated directly from the reaction mixture were examined by single crystal X-ray analysis. The copper clusters have a common structural motif that differs from either the cubane or the stairstep configurations, and is similar to that reported for a related complex with bridging $P^{\wedge}P$-type ligands, $Cu_4I_4(dcpm)_2$ (dcpm = bis(dicyclohexylphosphino)-methane).[40] Figure 2 shows the structure of cluster **3** as a representative example. Unlike cubane-type $Cu_4I_4L_4$ clusters (cf. Figure 1b), derivatives **1**−**5** all exhibit rigorous C_i crystallographic symmetry. The four copper atoms are arrayed

dx.doi.org/10.1021/ic2015226 | Inorg. Chem. 2012, 51, 230−236

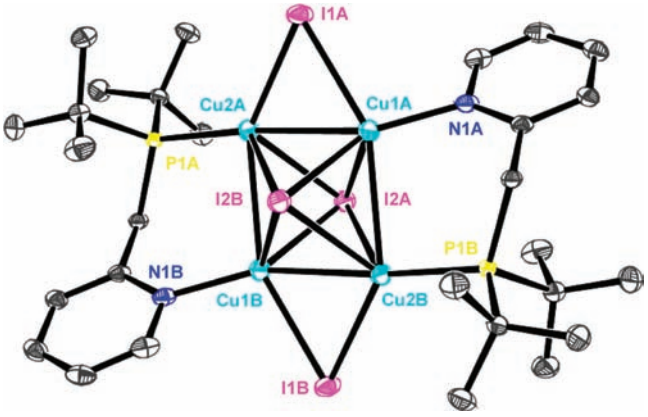

Figure 2. ORTEP drawing of the cluster **3** with ellipsoids at the 40% probability level, hydrogen atoms are omitted for clarity.

in a parallelogram with obtuse angles that vary from 90.81° for **1** to 98.50° for **5**. The Cu_4 array is μ^4-capped by two iodine atoms, which forms a distorted octahedron, and has two additional iodine atoms μ^2-bound on each short side of the parallelogram. The P^N-type ligands are coordinated to separate metals on opposing long sides of the Cu_4 array in a C2-symmetric arrangement. The Cu−N bond lengths range between 1.999−2.018 Å (average = 2.007(3) Å), while the Cu−P bond lengths fall between 2.209−2.237 Å (average = 2.220(1) Å) and are similar to the values observed in $Cu_4I_4(dcpm)_2$ (Cu−P = 2.218−2.224 Å).[40]

The Cu_4I_4 core structures of **1**−**5** are shown in Figure 3 along with selected bond distances. The clusters can be viewed as being composed of two Cu_2I_2 dimers (see Figure 1a), denoted A and B. The dimers are associated along their *Cu*−*Cu*−*I* faces such that their respective Cu−Cu axes are oriented in a parallel fashion (see Figure 1d) and have fold angles that range between 48.43° for **3** to 55.28° for **4**. The average distance between Cu and μ^2-bound iodide (2.651(1) Å) is markedly shorter than to the μ^4-bound iodide (2.725(1) Å). The Cu1A−Cu2A distances vary from 2.525(2) to 2.630(1) Å and are comparable to the equivalent Cu−Cu distance (2.576 Å) found in $Cu_4I_4(dcpm)_2$.[40] These Cu−Cu lengths are much shorter than those found in Cu_2I_2 clusters coordinated with monodentate N-heteroaromatic ligands (2.872−3.303 Å)[41] or diphosphine ligands (2.898 Å),[42] but are comparable with those in bimetallic complexes supported by 1,2,3-triazole (2.530 Å),[25] benzimidazoles (2.546 Å),[43] 2-benzoyl pyridines (2.587 Å),[44] 1,8-naphthyridine (2.61−2.63 Å),[45] and related nitrogen donor ligands.[46−51] The steric constraints imposed by the bridging P^N-ligands also influence the separation between A and B fragments in the five Cu_4I_4 cores. Compounds **3** and **4** have the shortest distance between Cu1A−Cu2B (2.839(3) and 2.880(1) Å, respectively), whereas the longest separation is found in **5** (3.035(2) Å). The latter value is similar to that reported for $Cu_4I_4(dcpm)_2$ with a P^P bridging ligand (Cu−Cu = 3.005(1) Å).[40] Likewise, short Cu(A)−I(B) distances are found in **3** (Cu1A−I2B = 2.647(1) Å) and **4** (Cu1A−I2B = 2.804(1) Å) while the longest value is seen in **5** (Cu2A−I2B = 3.249(2) Å).

The absorption spectra of the compounds **1**−**4**, recorded as saturated solutions in dichloromethane, as well as that of compound **5** are shown in Figure 4a. Compounds **2** and **3** have extremely poor solubility; their saturated solutions have maximum absorbance of only about 0.1, while those of the compounds **1** and **4** are about 0.9. The spectra, which resemble those reported for cubane $Cu_4I_4L_4$ clusters (L = pyridyl or organophosphine),[18,52] are characterized by a broad absorption band at 280 nm, assigned to ligand-centered transitions, and featureless transitions at longer wavelengths (>300 nm) that gradually decrease in intensity, assigned to halide-to-ligand charge-transfer transitions. The low energy transitions can be observed down to 430 nm in the excitation spectra recorded from neat solids (Figure 4a). Note though that the lineshapes of the excitation spectra do not parallel the absorption spectra at shorter wavelengths because of the strong self-absorption that occurs from the high molar concentration in the solid state samples.

Luminescence spectra for the clusters **1**−**5** recorded in the solid state at room temperature and 77 K, and in 2-MeTHF solution at 77 K, are shown in Figure 4b−d; data are summarized in Table 1. At room temperature, the clusters display varied luminescence with quantum yields (Φ_{PL}) ranging

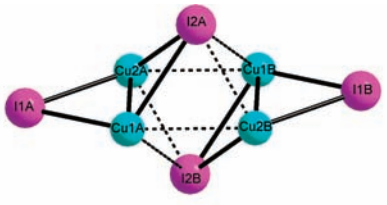

bond	1	2	3	4	5
Cu1A–I1A	2.646(1)	2.703(1)	2.712(1)	2.697(1)	2.682(2)
Cu2A–I1A	2.621(1)	2.609(1)	2.616(1)	2.613(1)	2.615(2)
Cu1A–I2A	2.751(1)	2.706(1)	2.815(2)	2.710(1)	2.697(1)
Cu2A–I2A	2.657(1)	2.690(1)	2.777(2)	2.820(1)	2.630(1)
Cu1A–Cu2A	2.525(2)	2.574(1)	2.630(1)	2.620(1)	2.562(2)
Cu1A–Cu2B	2.943(2)	2.930(1)	2.839(3)	2.880(1)	3.035(2)
Cu1A–I2B	2.872(1)	2.869(1)	2.647(2)	2.804(1)	2.812(2)
Cu2A–I2B	2.994(1)	2.986(1)	2.986(2)	2.833(1)	3.249(2)

Figure 3. Illustration of Cu_4I_4 core structure of the clusters **1**−**5**: Cu, cyan; I, purple. Inset table: selected bond distances (Å) in the five clusters.

dx.doi.org/10.1021/ic2015226 | *Inorg. Chem.* 2012, 51, 230−236

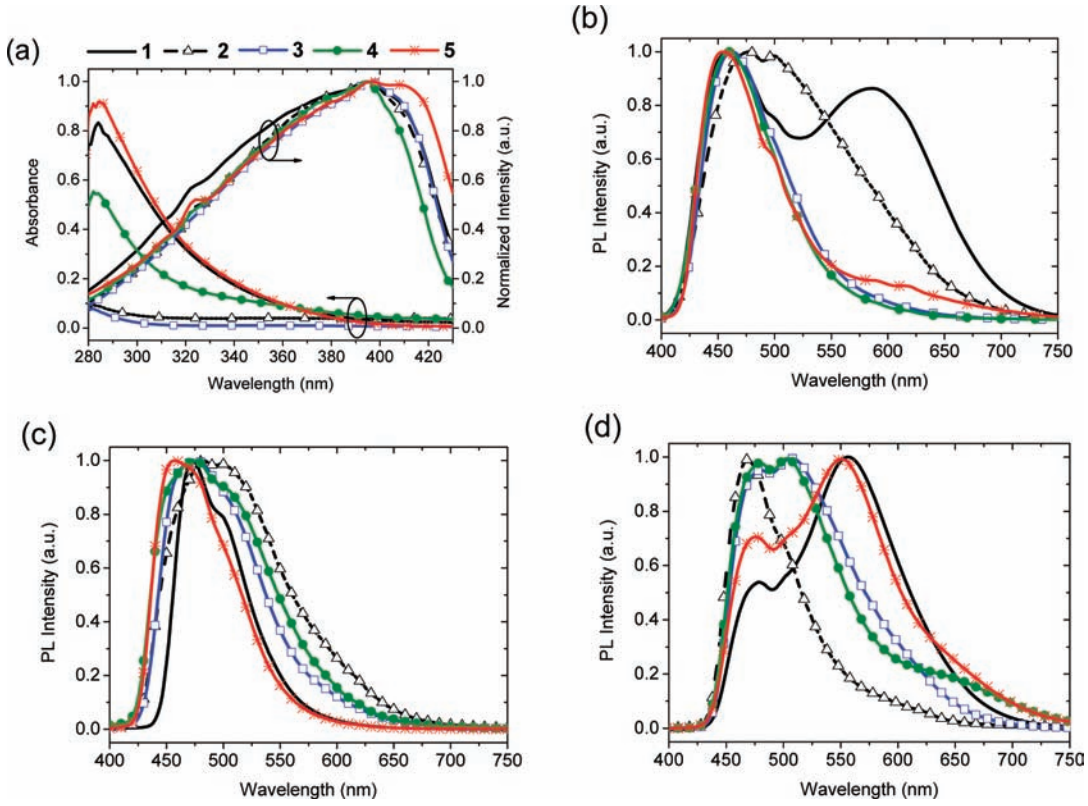

Figure 4. (a) Absorption spectra in dichloromethane solution for **1**−**5** along with excitation spectra in the solid state monitored at λ_{em} = 460 nm, (b−d) are normalized emission spectra at (b) room temperature in the solid state, (c) 77 K in the solid state, and (d) 77 K in 2-MeTHF solution. An excitation wavelength of 350 nm was used to record spectra (b−d).

Table 1. Photoluminescent Quantum Yield (Φ_{PL}), Peak Emission Wavelengths (λ_{em}), and Lifetime (τ) for Clusters 1−5

	crystalline powder (298 K)			crystalline powder (77 K)		2Me-THF solution (77 K)	
	Φ_{PL}	λ_{em} (nm)[a]	τ (μs)	λ_{em} (nm)	τ (μs)	λ_{em} (nm)[a]	τ (μs)
1	0.43	460/580	3.4/3.5	470	16.4	470/560	26.6/17.9
2	0.12	470/560	0.3, 1.4[b]/0.4, 5.9[c]	480	6.6, 18.8[d]	470	13.6
3	0.56	460	1.6	470	20.3	480/560	29.4/31.4
4	0.13	460	0.6, 5.5[e]	470	15.9	480/600	24.9/23.0
5	0.08	450/570	0.5/0.5, 2.4[f]	460	19.1	470/560	24.9/29.3

[a]The maxima for the emission band at lower energy were determined by Gaussian fitting. In the biexponential decays, the percentage of the longer lifetime is as found in the following five footnotes. [b]Percentage of the longer lifetime is 55%. [c]Percentage of the longer lifetime is 86%. [d]Percentage of the longer lifetime is 81%. [e]Percentage of the longer lifetime is 24%. [f]Percentage of the longer lifetime is 26%.

from 0.08 to 0.56 in microcrystalline powders. The five clusters can be divided into two categories on the basis of their emission spectra in the solid state (Figure 4b): the first group shows only a high energy (HE) emission band around 450−470 nm (**3** and **4**), while the second shows an additional low energy (LE) emission band (or shoulder) near 560−580 nm (**1**, **2**, and **5**). In the five clusters, both the HE and LE luminescence transients decay on the microsecond time scale (Table 1), implying that these transitions originate from triplet excited states. The emission spectra of **1**−**5** differ from that of $Cu_4I_4(dcpm)_2$, which only displays a LE emission band (λ_{em} = 590 nm, Φ_{PL} = 0.12, τ = 9.7 μs) at room temperature.[40] When the temperature is decreased to 77 K, no LE emission can be observed from clusters **1**, **2**, and **5** (Figure 4c). The luminescent thermochromism is most obvious for the cluster **1** (see Supporting Information), giving a blue emission at 77 K and white emission at room temperature that can be easily distinguished by the naked eye. The thermochromic behavior observed here is related to that displayed by the $Cu_4I_4(py)_4$[18] and $Cu_4I_4(dcpm)_2$[40] complexes, except that **1** shows dual emission at room temperature, whereas $Cu_4I_4(py)_4$ and $Cu_4I_4(dcpm)_2$ display only LE emission under the same conditions. Moreover, solid $Cu_4I_4(dcpm)_2$ displays almost equal amounts of HE (λ_{em} = 490 nm) and LE (λ_{em} = 650 nm) emission at 77 K.[40] In 2-MeTHF solution clusters **1**−**5** are nonemissive at room temperature, but bright luminescence is observed at 77 K (Figure 4d). Clusters **3** and **4** display broad emission centered at 500 nm with shoulders near 560 and 600 nm, respectively. Clusters **1** and **5** show dual emission bands around 470 and 560 nm that are red-shifted and blue-shifted, respectively, compared with their emission in the solid state at room temperature. The cluster **2** gives an HE emission band at 470 nm along with a much weaker LE emission shoulder near 570 nm.

To gain insight into the emission properties, we performed single-point DFT calculations of **1**−**5** using coordinates

dx.doi.org/10.1021/ic2015226 | Inorg. Chem. 2012, 51, 230−236

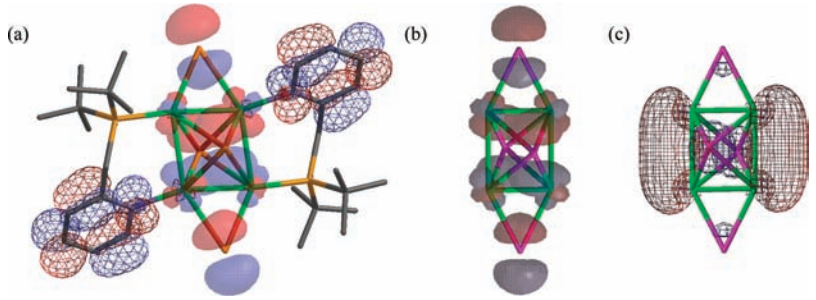

Figure 5. HOMO (transparent) and LUMO (mesh) frontier orbitals plots for the cluster **3** (a), and for the HOMO (b) and LUMO (c) of octahedral Cu_4I_4.

obtained from the X-ray analyses. Calculations were also performed on bare Cu_4I_4 clusters that were energy minimized in both the cubane and the octahedral geometries. Theoretical investigations of this type have proven to be very helpful in establishing the nature of the highest occupied molecular orbital (HOMO) and the lowest unoccupied molecular orbital (LUMO) of related copper complexes and aided in the assignment of spectral transitions.[13,17,52−54] The calculations were performed with the Titan software package using a B3LYP/LACVP** model. The five clusters have similar frontier orbitals; Figure 5a shows representative HOMO and LUMO plots for **3** (see Supporting Information for MO images of the other clusters). As shown in the figure, the HOMOs are mainly localized on the iodide 5p (48%) and copper 3d (43%) orbitals, while the LUMOs are almost exclusively on the pyridyl groups (82%) with minor participation from orbitals on the Cu (7.7%) and P (4.4%) atoms. The contribution of these atomic orbitals to the electronic structure of the HOMO is similar to that described for cubane derivatives, $Cu_4I_4(PH_3)_4$.[53] A calculation of the bare octahedral Cu_4I_4 cluster shows that the energy, minimized without constraints, is 65.85 kcal/mol higher than that of the bare Cu_4I_4 cubane. The Cu−I distances for the μ^2 (2.662 Å) and μ^4 (2.873 and 2.888 Å) interactions compare favorably to the corresponding bonds found in **1**−**5**, while the Cu−Cu distances similarly have short (2.479 Å, μ^2-bound) and long (2.986 Å) separations. The HOMO of the bare octahedral Cu_4I_4 (Figure 5b) has an electronic structure equivalent to that of **3** and is composed primarily of iodide 6p orbitals (53.3%) and Cu 3d orbitals (41.3%) arranged in an antibonding configuration. The LUMO (Figure 5c) consists of orbitals on the iodide (6s, 36.2%; 6p, 17.5%) and Cu (4s, 34.9%; 4p, 10.7%; 3d, 0.07%) atoms and shows a net bonding interaction between the Cu pair with long separation. For the calculated structure of the triplet state of the bare octahedral Cu_4I_4, the Cu−Cu distances for the μ^2-bound copper atoms expand to 2.682 Å, whereas the nonbridged Cu−Cu distances contract to 2.566 Å. On the other hand, distances for the Cu−I μ^2 (2.676 Å) and μ^4 (2.895 and 2.899 Å) interactions are only slightly longer than in the singlet ground state. The change in the Cu_4 framework in the bare cluster is likely due to population of σ-bonding 4s and 4p orbitals of the LUMO in the cluster centered triplet (^{3}CC) state.

For clusters **1**−**5** the π-orbitals of the pyridyl ligands have lower energies than the 4s, 4p σ-bonding combinations; thus a halide-to-ligand charge transfer (XLCT) transition is the lowest energy excited state when the complexes are in the ground state geometry. Unoccupied molecular orbitals with significant 4s character on the Cu atoms (8−10%) only appear in LUMO+4. However, a previous DFT and time-dependent DFT (TDDFT) investigation of cubane $Cu_4I_4L_4$ (L = pyridyl, organophosphine) clusters proposed that both ^{3}XLCT and ^{3}CC states can still be populated upon irradiation at room temperature.[13,52] Excitation to the ^{3}XLCT state leaves the cluster structure relatively unperturbed, whereas the Cu_4I_4 core in the ^{3}CC configuration is significantly distorted from the ground state geometry since this transition is characterized by a net transfer of an electron from a set of antibonding 3d-orbitals to a bonding combination of 4s-orbitals.[52−54] The dual emission, thermochromic, and rigidochromic behavior of the $Cu_4I_4L_4$ clusters was explained by suggesting that the two electronic configurations are separated by an energy barrier and therefore, poorly coupled in the excited state at low temperatures. The ^{3}CC state can only be thermally populated at higher temperatures, which then leads to the observation of dual emission. Thus, by analogy, the HE emission bands at 450−470 nm observed in clusters **1**−**5** can be ascribed to transitions from an ^{3}XLCT configuration. The LE emissions observed from **1**, **2**, and **5** in the solid state at room temperature, and from **3** and **4** at 77 K in 2-MeTHF solution, are assigned to a distorted Cu_4I_4 based ^{3}CC configuration. The same assignments can be made to the equivalent HE and LE transitions reported for $Cu_4I_4(dcpm)_2$.[40]

While the luminescence from the **1**−**5** displays characteristics similar to the ^{3}XLCT and ^{3}CC emission reported for cubane $Cu_4I_4L_4$ complexes, the thermochromic and ridigochromic response of these two types of clusters are notably different. The predominant blue luminescence observed from compounds **1**−**5** at room temperature is in sharp contrast from the near exclusive green-to-orange emission seen from cubane $Cu_4I_4L_4$ complexes under the same conditions. The variation in the emissive behavior of **1**−**5** can be attributed to the effects of unequal Cu−Cu bond lengths in the Cu_4 array and to the rigid coordination environment enforced by the bidentate P^N ligands that stabilizes the molecular geometry in the ^{3}XLCT state. It has been shown that the Cu−Cu interactions in cubane $Cu_4I_4L_4$ clusters, as estimated from Cu−Cu distances, are the key parameter that influences the luminescence properties of the ^{3}CC transition.[52,55] For cubanes with pyridine based ligands that show strong ^{3}CC transitions, the reported Cu−Cu distances are in the range of 2.56−2.90 Å.[10,56] However, cubane derivatives with pyridyl[57,58] or phosphine[52] based ligands and Cu−Cu distances >2.90 Å can also display ^{3}CC transitions in the solid state at room temperature. Likewise, there is a correlation between the presence of the ^{3}CC emission band in clusters **1**−**5** and the Cu−Cu distances in the crystal structures. The three compounds that have the shortest Cu1A−Cu2A distances *within* the dimer unit (2.525(2), 2.574(1), and 2.562(2) Å for **1**, **2**, and **5**, respectively) show ^{3}XLCT and

dx.doi.org/10.1021/ic2015226 | *Inorg. Chem.* 2012, 51, 230−236

variable amounts of ^{3}CC emission at both room temperature and 150 K (the temperature at which the crystal structures were collected, see Supporting Information). However, these derivatives also have the longest Cu1A−Cu2B separation *between* dimer units (2.943(1), 2.930(1), and 3.035(2) Å for **1**, **2**, and **5**, respectively). Moreover, changes in just one pair of Cu−Cu distances are insufficient to account for the LE emission since clusters **3** and **4**, which exhibit little-to-no LE emission, also have short Cu1A−Cu2A separations that fall within the range found for ^{3}CC transitions. Since both theoretical[13] and experimental[55] studies of the cubane clusters, along with calculations of bare octahedral Cu_4I_4 (vida supra), show that the Cu(A)−Cu(B) distances significantly decrease when promoted to the ^{3}CC excited state, the overall geometry of the Cu_4I_4 core in **1**, **2**, and **5** must undergo some kind of structural relaxation to produce the LE emission. For example, a contraction of the longer Cu(A)−Cu(B) distances in the Cu_4 array of **1**, **2**, and **5** would entail a concomitant deformation of the bridging P^N ligand to accommodate the shortened Cu−Cu bonds. Any distortion of the P^N ligand would likely be influenced by the steric bulk of the organophosphine moiety. Thus, the presence of LE emission in **1**, **2**, and **5**, and conversely the relative absence in **3** and **4** (with bulky *tert*-butyl and *iso*-propyl groups), appears to be controlled by the extent to which the P^N ligand can warp and thereby allow the Cu_4 framework to relax during formation of the excited state.

The thermal stability of **1**−**5** with respect to vapor deposition under vacuum was examined by gradient sublimation at low pressure (10^{-6} Torr). None of the clusters could be sublimed intact. However, it is interesting to note that a binuclear complex **3a** is obtained during the sublimation of the cluster **3**. Moreover, sublimation of the complex **3a** gave a mixture of **3** and **3a**, indicating that there is a thermal equilibrium between the two species in the gas phase. Figure 6 shows an ORTEP of

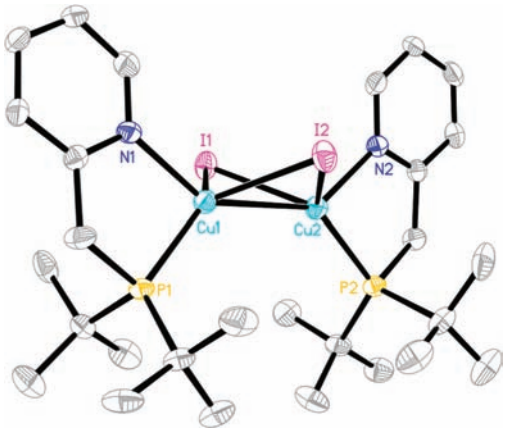

Figure 6. ORTEP drawing of the complex **3a** with ellipsoids at the 40% probability level. Hydrogen atoms are omitted for clarity. Selected distances (Å): Cu1−Cu2, 2.795(1); Cu1−P1, 2.234(1); Cu1−N1, 2.124(3); Cu1−I1, 2.636(1); Cu1−I2, 2.595(1); Cu2−N2, 2.126(3); Cu2−P2, 2.242(1); Cu2−I1, 2.641(1); Cu2−I2, 2.660(1).

the dimeric complex **3a**. Each Cu ion in **3a** has a distorted tetrahedral geometry and is coordinated by the bidentate P^N ligand along with two bridging μ^2-I atoms. The Cu−Cu (2.795(1) Å) and Cu−N (2.124(3) Å) distances are significantly longer than the respective values in cluster **3** (2.630 (1) and 2.018 (3) Å).

Complex **3a** displays a strong green luminescence centered at 530 nm (Φ_{PL} = 0.32, τ = 13 μs) in the solid state at room temperature (Figure 7). This emission is significantly red-

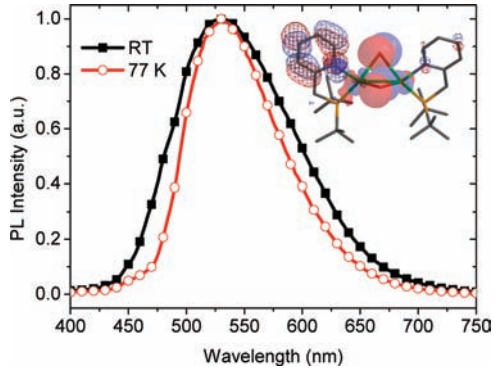

Figure 7. Emission spectra of **3a** in solid state at room temperature and 77 K. Inset: HOMO (transparent) and LUMO (mesh) plots for the dimeric complex **3a**.

shifted compared with luminescence from cluster **3** (λ_{em} = 460 nm), but comparable to that from the dimeric complex $Cu_2I_2(py)_4$ (λ_{em} = 517 nm).[18] At 77 K, the emission maximum of **3a** is unchanged but the bandwidth narrows and the lifetime increases to 38 μs. On the basis of DFT calculations (Figure 7, inset) and similarity to the HE photophysical properties from clusters **1**−**5**, the emission of the complex **3a** is assigned to a ^{3}XLCT transition.

SUMMARY

Five tetranuclear copper(I) iodide complexes with the formula $Cu_4I_4(P^N)_2$ (P^N = 2-[(di**R**phosphino)methyl]pyridine; **1**, R = phenyl; **2**, R = cyclohexyl; **3**, R = *t*-butyl; **4**, R = *i*-propyl; **5**, R = ethyl) have been synthesized. Structural characterization shows that **1**−**5** adopt a octahedral geometry for the Cu_4I_4 core, which has been rarely reported, that differs from the well-known cubane and stairstep configurations. The Cu−Cu bond lengths in the core of the Cu_4 array of **1**−**5** have both short (bridged by an μ^2-iodide) and long (flanked by the P^N ligands) separations. Photophysical studies show that the emission from this type cluster can be tuned from blue to white in the solid state at room temperature by utilizing P^N-type ligands with differing steric demands of the organophosphine group. DFT calculations suggest that P^N ligands serve to constrain relaxation of the long Cu−Cu distances in the Cu_4I_4 core during formation of the excited state. Thermal decomposition of cluster **3** occurs during sublimation and leads to the formation of a dinuclear complex, $Cu_2I_2(P^N)_2$ **3a**, which has been structurally and photophysically characterized.

ASSOCIATED CONTENT

Supporting Information

Crystallographic data in CIF format and summary of X-ray data collection and refinement of the clusters **1**−**5**, and the dimer complex **3a**; temperature dependent photoluminescence spectra for the cluster **1**; the DFT calculated HOMOs and LUMOs of clusters **1**, **2**, **4**, and **5**; photoluminescence spectra for the clusters **1**−**5** at 150 K. This material is available free of charge via the Internet at http://pubs.acs.org.

dx.doi.org/10.1021/ic2015226 | *Inorg. Chem.* 2012, 51, 230−236

AUTHOR INFORMATION

Corresponding Author
*E-mail: met@usc.edu.

ACKNOWLEDGMENTS

We wish to acknowledge Universal Display Corporation for financial support of this work.

REFERENCES

(1) Ford, P. C.; Cariati, E.; Bourassa, J. *Chem. Rev.* **1999**, *99*, 3625−3647.
(2) Armaroli, N.; Accorsi, G.; Cardinali, F.; Listorti, A. *Top. Curr. Chem.* **2007**, *280*, 69−115.
(3) Perruchas, S.; Le Goff, X. F.; Maron, S.; Maurin, I.; Guillen, F.; Garcia, A.; Gacoin, T.; Boilot, J. P. *J. Am. Chem. Soc.* **2010**, *132*, 10967−10969.
(4) Deaton, J. C.; Switalski, S. C.; Kondakov, D. Y.; Young, R. H.; Pawlik, T. D.; Giesen, D. J.; Harkins, S. B.; Miller, A. J. M.; Mickenberg, S. F.; Peters, J. C. *J. Am. Chem. Soc.* **2010**, *132*, 9499−9508.
(5) Liu, Z. W.; Qayyum, M. F.; Wu, C.; Whited, M. T.; Djurovich, P. I.; Hodgson, K. O.; Hedman, B.; Solomon, E. I.; Thompson, M. E. *J. Am. Chem. Soc.* **2011**, *133*, 3700−3703.
(6) Kamigaito, M.; Ando, T.; Sawamoto, M. *Chem. Rev.* **2001**, *101*, 3689−3745.
(7) Fache, F.; Schulz, E.; Tommasino, M. L.; Lemaire, M. *Chem. Rev.* **2000**, *100*, 2159−2231.
(8) McMillin, D. R.; McNett, K. M. *Chem. Rev.* **1998**, *98*, 1201−1219.
(9) Dyason, J. C.; Healy, P. C.; Pakawatchai, C.; Patrick, V. A.; White, A. H. *Inorg. Chem.* **1985**, *24*, 1957−1960.
(10) Raston, C. L.; White, A. H. *Dalton Trans.* **1976**, 2153−2156.
(11) Rath, N. P.; Maxwell, J. L.; Holt, E. M. *Dalton Trans.* **1986**, 2449−2453.
(12) Eitel, E.; Oelkrug, D.; Hiller, W.; Strahle, J. *Z. Naturforsch. B* **1980**, *35*, 1247−1253.
(13) De Angelis, F.; Fantacci, S.; Sgamellotti, A.; Cariati, E.; Ugo, R.; Ford, P. C. *Inorg. Chem.* **2006**, *45*, 10576−10584.
(14) Omary, M. A.; Mohamed, A. A.; Rawashdeh-Omary, M. A.; Fackler, J. P. *Coord. Chem. Rev.* **2005**, *249*, 1372−1381.
(15) Dias, H. V. R.; Diyabalanage, H. V. K.; Eldabaja, M. G.; Elbjeirami, O.; Rawashdeh-Omary, M. A.; Omary, M. A. *J. Am. Chem. Soc.* **2005**, *127*, 7489−7501.
(16) Lo, W. Y.; Lam, C. H.; Yam, V. W. W.; Zhu, N. Y.; Cheung, K. K.; Fathallah, S.; Messaoudi, S.; Le Guennic, B.; Kahlal, S.; Halet, J. F. *J. Am. Chem. Soc.* **2004**, *126*, 7300−7310.
(17) Vitale, M.; Palke, W. E.; Ford, P. C. *J. Phys. Chem.* **1992**, *96*, 8329−8336.
(18) Kyle, K. R.; Ryu, C. K.; DiBenedetto, J. A.; Ford, P. C. *J. Am. Chem. Soc.* **1991**, *113*, 2954−2965.
(19) Ford, P. C.; Vogler, A. *Acc. Chem. Res.* **1993**, *26*, 220−226.
(20) Ford, P. C. *Coord. Chem. Rev.* **1994**, *132*, 129−140.
(21) Bondi, A. *J. Phys. Chem.* **1964**, *68*, 441−451.
(22) Batsanov, S. S. *Inorg. Mater.* **2001**, *37*, 871−885.
(23) Nag, S.; Banerjee, K.; Datta, D. *New J. Chem.* **2007**, *31*, 832−834.
(24) Filatov, A. S.; Hietsoi, O.; Sevryugina, Y.; Gerasimchuk, N. N.; Petrukhina, M. A. *Inorg. Chem.* **2010**, *49*, 1626−1633.
(25) Su, C. Y.; Kang, B. S.; Sun, J. *Chem. Lett.* **1997**, *26*, 821−822.
(26) Ma, Z. C.; Xian, H. S. *J. Chem. Crystallogr.* **2006**, *36*, 129−133.
(27) Song, R. F.; Xie, Y. B.; Li, J. R.; Bu, X. H. *CrystEngComm* **2005**, *7*, 249−254.
(28) Samanamu, C. R.; Lococo, P. M.; Woodul, W. D.; Richards, A. F. *Polyhedron* **2008**, *27*, 1463−1470.
(29) Manbeck, G. F.; Brennessel, W. W.; Evans, C. M.; Eisenberg, R. *Inorg. Chem.* **2010**, *49*, 2834−2843.
(30) Healy, P. C.; Pakawatchai, C.; Raston, C. L.; Skelton, B. W.; White, A. H. *Dalton Trans.* **1983**, 1905−1916.
(31) Cariati, E.; Roberto, D.; Ugo, R.; Ford, P. C.; Galli, S.; Sironi, A. *Inorg. Chem.* **2005**, *44*, 4077−4085.
(32) Lee, C. S.; Wu, C. Y.; Hwang, W. S.; Dinda, J. *Polyhedron* **2006**, *25*, 1791−1801.
(33) Mochida, T.; Okazawa, K.; Horikoshi, R. *Dalton Trans.* **2006**, 693−704.
(34) Diez, J.; Gamasa, M. P.; Panera, M. *Inorg. Chem.* **2006**, *45*, 10043−10045.
(35) Xie, Y. B.; Ma, Z. C.; Wang, D. *J. Mol. Struct.* **2006**, *784*, 93−97.
(36) Peng, R.; Li, D.; Wu, T.; Zhou, X. P.; Ng, S. W. *Inorg. Chem.* **2006**, *45*, 4035−4046.
(37) Carlson, B.; Eichinger, B. E.; Kaminsky, W.; Phelan, G. D. *J. Phys. Chem. C* **2008**, *112*, 7858−7865.
(38) Braunstein, P.; Heaton, B. T.; Jacob, C.; Manzi, L.; Morise, X. *Dalton Trans.* **2003**, 1396−1401.
(39) Hung-Low, F.; Klausmeyer, K. K. *Inorg. Chim. Acta* **2008**, *361*, 1298−1310.
(40) Fu, W. F.; Gan, X.; Che, C. M.; Cao, Q. Y.; Zhou, Z. Y.; Zhu, N. N. Y. *Chem.—Eur. J.* **2004**, *10*, 2228−2236.
(41) Araki, H.; Tsuge, K.; Sasaki, Y.; Ishizaka, S.; Kitamura, N. *Inorg. Chem.* **2005**, *44*, 9667−9675.
(42) Tsuboyama, A.; Kuge, K.; Furugori, M.; Okada, S.; Hoshino, M.; Ueno, K. *Inorg. Chem.* **2007**, *46*, 1992−2001.
(43) Toth, A.; Floriani, C.; Chiesivilla, A.; Guastini, C. *Inorg. Chem.* **1987**, *26*, 3897−3902.
(44) Goher, M. A. S.; Abdou, A. E. H.; Yip, W. H.; Mak, T. C. W. *Polyhedron* **1993**, *12*, 2981−2987.
(45) Araki, H.; Tsuge, K.; Sasaki, Y.; Ishizaka, S.; Kitamura, N. *Inorg. Chem.* **2007**, *46*, 10032−10034.
(46) Healy, P. C.; Kildea, J. D.; Skelton, B. W.; White, A. H. *Aust. J. Chem.* **1989**, *42*, 115−136.
(47) Oshio, H.; Watanabe, T.; Ohto, A.; Ito, T.; Masuda, H. *Inorg. Chem.* **1996**, *35*, 472−479.
(48) Healy, P. C.; Pakawatchai, C.; White, A. H. *Dalton Trans.* **1985**, 2531−2539.
(49) Ramos, J.; Yartsev, V. M.; Golhen, S.; Ouahab, L.; Delhaes, P. *J. Mater. Chem.* **1997**, *7*, 1313−1319.
(50) Engelhardt, L. M.; Healy, P. C.; Skelton, B. W.; White, A. H. *Aust. J. Chem.* **1988**, *41*, 839−844.
(51) Belsky, V. K.; Ishchenko, V. M.; Bulychev, B. M.; Soloveichik, G. L. *Polyhedron* **1984**, *3*, 749−752.
(52) Perruchas, S.; Tard, C.; Le Goff, X. F.; Fargues, A.; Garcia, A.; Kahlal, S.; Saillard, J. Y.; Gacoin, T.; Boilot, J. P. *Inorg. Chem.* **2011**, *50*, 10682−10692.
(53) Vitale, M.; Ryu, C. K.; Palke, W. E.; Ford, P. C. *Inorg. Chem.* **1994**, *33*, 561−566.
(54) Vega, A.; Saillard, J. Y. *Inorg. Chem.* **2004**, *43*, 4012−4018.
(55) Kitagawa, H.; Ozawa, Y.; Toriumi, K. *Chem. Commun.* **2010**, *46*, 6302−6304.
(56) Ren, S. B.; Zhou, L.; Zhang, J.; Li, Y. Z.; Du, H. B.; You, X. Z. *CrystEngComm* **2009**, *11*, 1834−1836.
(57) Ryu, C. K.; Vitale, M.; Ford, P. C. *Inorg. Chem.* **1993**, *32*, 869−874.
(58) Engelhardt, L. M.; Healy, P. C.; Kildea, J. D.; White, A. H. *Aust. J. Chem.* **1989**, *42*, 107−113.